Internal Waves Generated from Asymmetric Topographies

Kyle Hakes
Brigham Young University

Dr. Julie Crockett
Brigham Young University

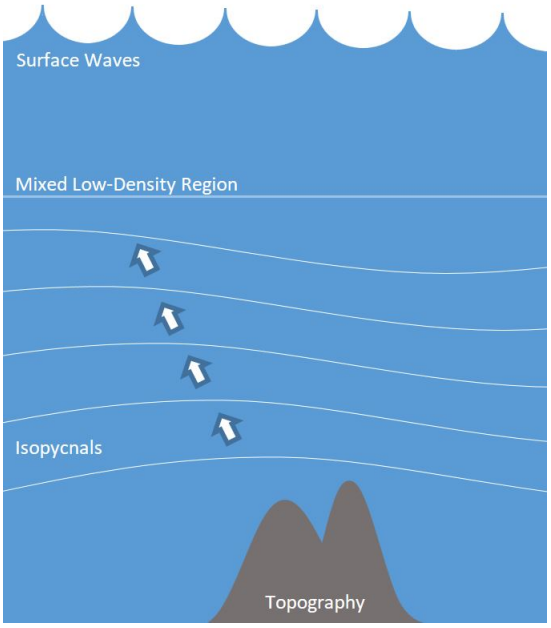

Fig. 1. Tidally generated internal waves in the ocean

Internal waves are a key part of the energy budget of the ocean and atmosphere. The generation of internal waves in the ocean from tides is dependent on the frequency of oscillation, the profile of the underwater mountain range, and the density of water in the surrounding ocean. A study of the effect of an asymmetric mountain range, with varying profiles, on the generation of internal waves is presented. Results begin to indicate that the wave is mostly similar when generated on either side of the topography, but might extend to higher wavenumbers in Fourier space when generated on the wide side.

1 Introduction

Internal waves are generated in stratified fluids such as the ocean and atmosphere. In the ocean, internal waves are some of the most energetic events and significantly affect the mixing and energy budget. In a stratified fluid like the ocean, the density varies with depth. When a stable stratification is disturbed, internal waves can be generated. In the ocean, the tides oscillating water back and forth over underwater mountain ranges can generate internal waves. Figure 1 shows a representation of internal waves being generated from oceanic topography. Near the free surface there is a mixed, low-density region caused by surface disturbances such as wind and waves, but as depth increases, a consistently increasing density profile can be observed. Isopycnal lines, or lines of constant density, are shown to visualize the changing density and wave motion. These waves are different from free surface waves as they are wholly contained inside the ocean. The propagation of these tidally generated internal waves depends on the frequency of oscillation (ω), the profile of the mountain range, and the density stratification profile in the surrounding ocean (N).

Internal waves transport energy from their point of generation to other parts of the ocean or atmosphere where they can subsequently break and mix their local surroundings, allowing vertical transport of heat and nutrients [1]. The mixing of these nutrients is essential to the survival of life in the ocean. Just as a stagnant pond cannot support diverse forms of life, the ocean must be constantly mixed in order to support the vast array of life present. Furthermore, internal waves can affect weather patterns by causing storms to form or break up unexpectedly, and generate clear air turbulence, affecting flight patterns. Internal waves must be further researched to improve understanding and predictability of these events.

Experiments, observations, and simulations are often used to study internal waves. Experiments allow the control of variables, and can be performed at a fraction of the cost of observations, although realistic topography can be tough to characterize. When realistic topographies are scaled down the impact of minor features is lost and only the effect of major features can be determined. In addition, smoothed topographies with analytical solutions are often used in order to compare with expected values from theory [2]. One of the most common experimental methods is Synthetic Schlieren

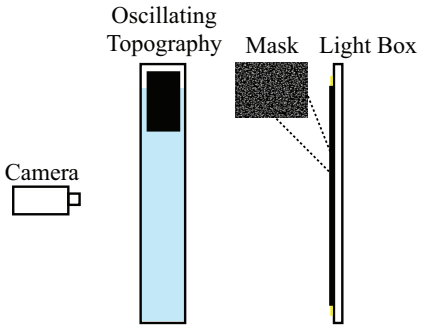

Fig. 2. a) Synthetic schlieren experimental setup side view b) View from the camera c) Sample output

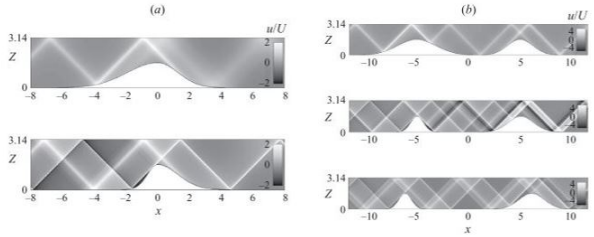

Fig. 3. a) Asymmetric topographies b) Varying double ridge topographies where the middle and bottom images have the same topographies, but varied distance between the ridges

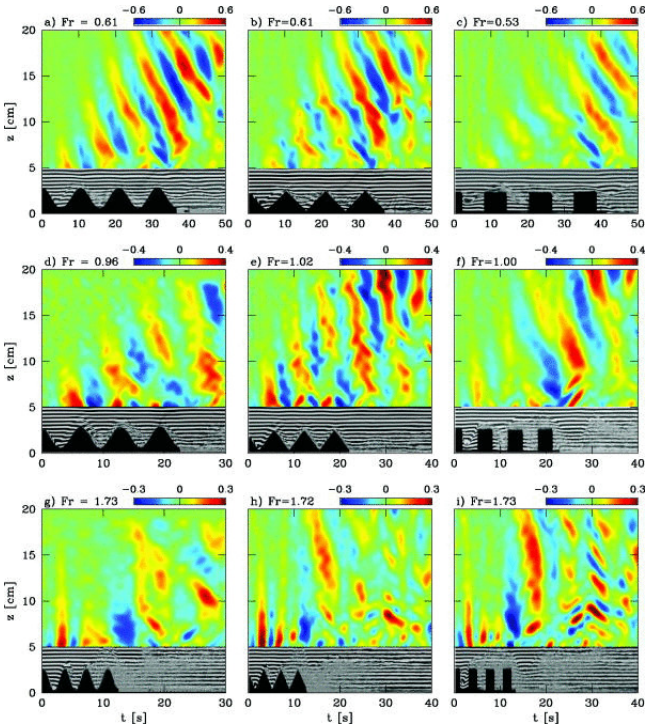

Fig. 4. (Color) Vertical time series of N^2 for the sinusoidal, triangular, and rectangular hills at three different Fr. The raw images are attached below each test to help visualize the position of the topographies and their motion.

(SS). Synthetic Schlieren takes advantage of the dependence of the refraction of light through water of different salinities, and thus density [3]. An example of SS imaging setup and results is shown in Fig. 2. Fig. 2a shows a typical SS setup where a camera looks through a tank to view an illuminated mask of dots. A sample image from the camera is shown in Fig. 2b and in Fig. 2c a processed image is shown where the wave beams can be seen propagating away from the topography. Further details of SS are explained in Section 2.

Previously, SS has been used to investigate the generation of internal waves over Gaussian, knife edge and complex topographic shapes [4, 5]. Observations and simulations have looked at the same topographies, as well as sloped, shelf, trench, and double ridge topographies [6, 7]. Numerical simulations have been presented for specific asymmetric topographies for a uniform flow such as a flood or ebb tide [8]. The waves propagating from these asymmetric topographies differ from those generated from symmetric topographies, due to their reliance on the direction of the tidal flow. Despite having similar shapes and flow conditions, the waves propagating from these asymmetric topographies generate different waves based on the amplitude of their slopes. Experiments have lagged behind observations and simulations in investigating more complicated topographies, such as asymmetric profiles, but a few exist. Confined, repeating, linear waves, known as wave attractors, have been studied between asymmetric topographies and double ridges, both using simulations and Particle Image Velocimetry experiments [9]. In Fig. 3 the velocity field (u/U) is shown as tidal flow is oscillated over ridges [9]. The topographies extend to half the water depth and the waves reflect between the topography, bottom of the tank, and the surface of the water. This confinement allows the convenient visualization of wave attractors, but not the propagation of individual internal waves. However, the effect of topographic asymmetry can be observed in Fig. 3a as the wave attractors on the left and right of the topography differ from each other. Furthermore, when looking at double ridges in Fig. 3b, interaction can be seen between the two ridges that varies based on the spacing between them and their slopes.

The effect of topographic slope on internal waves has been studied previously, with both singular and repeating topographies. Calculations were performed for both isolated triangular and polynomial topographies with equivalent amplitudes but differing slopes [10]. The energy flux varied significantly based on the different slopes of the ridges. Experiments have been also performed that looked at the types of waves generated from sinusoidal, triangular, and rectangular hill groups [11]. The topographies consisted of four hills of equivalent amplitudes, and three different lengths were used for comparison as seen in 4, where separation distance decreases moving top to bottom. The colored images are processed results from SS, and the black and white show the topographies and SS mask for reference. As the distance between ridges decreases and the steepness of the ridges increases, internal waves become less distinct, and the angle of propagation can no longer be visually discerned. The ridges begin to act more as a singular topography than a row of distinct ones as the distance between them closes.

a_t	b_t	c_t	Case
1.0	0	1.0	Medium
1.0	0	0.5	Steep
0.8	0.25	2.0	Wide 1
0.8	0.25	2.0	Wide 2

Table 1. Defining dimensions for the topographies

It has been observed that asymmetry of oceanic topography can affect the generation of internal waves [8, 9], and the severity of topographic slope and proximity of different ridges can also have a distinct impact on internal wave generation [11].

2 Methods

Four asymmetric topographies were designed in CAD and 3D printed, similar to topographies currently used in the Stratified Flow lab. The topographies are depicted in Fig. 5 and Table 1 and are defined by overlapping a wide Gaussian profile over a medium and steep Gaussian profile [12] that is defined by

$$y = a_t e^{-(x-b_t)^2/c_t^2} \tag{1}$$

where a_t is the amplitude of the topography, b_t is the offset, and c_t defines the spread as a multiple of the spread of the medium topography. The combination of a medium and steep topography results in a topography with two distinctly different sides.

Experiments were conducted by filling the narrow tank using a version of the double bucket method [13], to create a constant N profile with density defined by

$$\rho = dz + e \tag{2}$$

and N defined by

$$N = \sqrt{-gd/\rho_o} \tag{3}$$

with d and e being constants, z being the depth of water, g is gravity, and ρ_o is the initial density of water. Near the surface, the water is less dense, and increases in density with depth. A topography is inverted and placed at the surface of the tank, as shown in Figure 2. The topography is then oscillated back and forth, creating internal waves. A matrix of dots (mask) is illuminated behind the tank and as the internal waves move through the tank, from the perspective of the camera, the dots move, allowing visualization of the waves. To allow the internal waves to reach a steady state, the topography is oscillated for 15 periods. Using commercially available Digiflow software, three minutes of images

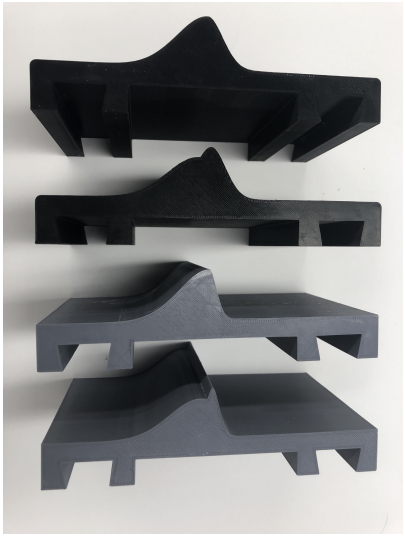

Fig. 5. Topographies used for experiments. From top to bottom numbered 1-4

Topography	Frequency	Side
1	High	Asymmetric
1	High	Normal
1	Low	Asymmetric
1	Low	Normal
2	High	Asymmetric
2	High	Normal
2	Low	Asymmetric
2	Low	Normal
⋮	⋮	⋮
4	Low	Normal

Table 2. Experimental test list

are captured at 6 fps. In between tests, the tank is allowed to rest for 20 minutes in order to allow the water to settle back to its undisturbed state. Images of the waves generated from both the asymmetric and normal sides of the topography were imaged. Topographies are oscillated at both a high (0.9 N) and a low (0.7 N) frequency. Experiments resemble tests that have been completed previously using symmetric topographic profiles by the Stratified Flow Lab in both relative frequency and density profile. For comparison, the generalized list of experiments is outlined in Table 2.

Experimental data from SS ($d\rho/dz$) combined with the measured density profile of the tank is analyzed to estimate the kinetic energy of the internal wave, the shape and beam angle, and the spread of the wave across frequencies and wavenumbers. Digiflow analyzes the images and outputs values of ΔN^2 which indicates how the natural frequency has changed relative to the undisturbed state, which allows vi-

sualization of internal wave propagation. This output is then processed in Matlab, utilizing Fourier analysis to estimate kinetic energy, following the process outlined by Wunsch and Brandt [14]. Kinetic energy is calculated using the horizontal and vertical velocities, u and w

$$KE = u^2 + w^2 \tag{4}$$

and the velocities and natural frequency are defined as

$$u(x,z,t) = \int \tilde{U} \exp[i(kx + mz - \omega t)] \mathrm{d}k\mathrm{d}\omega \tag{5}$$

$$w(x,z,t) = \int \tilde{W} \exp[i(kx + mz - \omega t)] \mathrm{d}k\mathrm{d}\omega \tag{6}$$

$$\Delta N^2(x,z,t) = \int \Delta\tilde{N^2} \exp[i(kx + mz - \omega t)] \mathrm{d}k\mathrm{d}\omega \tag{7}$$

where $\tilde{U}$, $\tilde{W}$ and $\Delta\tilde{N^2}$ are Fourier amplitudes of a 2D Fourier transform through time and (x) and the vertical and horizontal wavenumbers are m and k respectively. Using the continuity equation

$$\frac{\partial u}{\partial x} + \frac{\partial w}{\partial z} = 0 \tag{8}$$

and defining

$$\frac{\partial \Delta N^2}{\partial t} = -\frac{\partial (N^2 w)}{\partial z} \tag{9}$$

with Eqs. 5-7 and assuming that the derivatives of the amplitudes are negligible, the kinetic energy can be estimated

$$KE_2 = \frac{\omega^2 N^2}{k^2(N^2 - \omega^2) + (\omega \partial_z N^2 / N^2)^2} \left| \frac{\Delta\tilde{N^2}}{N^2} \right|^2 \tag{10}$$

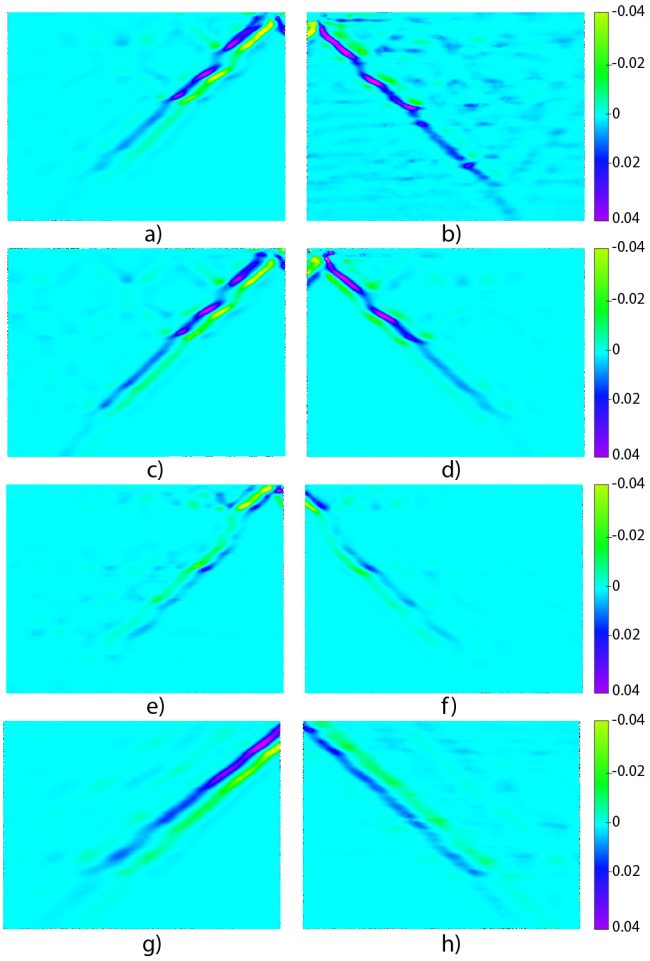

Fig. 6. Raw data for topographies 1-4, from top to bottom, with the left column being medium for the first two rows and steep for the last two rows, while the right column is always the wide side

3 Results

Synthetic Schlieren tests were completed with all four topographies listed in 1, and shown in Fig. 5. Each test imaged either the medium/steep or the wide side of the topography, and was conducted at a low or high frequency. The generated wave from the two sides will be compared first qualitatively, then quantitatively. The results were similar at both the low and high frequencies and thus only the low frequency wave will be discussed.

In Fig. 6 the raw data from Digiflow of ΔN^2 is displayed. The topography is located in the top right of the left column of images, and the top left of the right column of images. Change in N^2 is represented by the colors where negative values are troughs and positive values are crests, which move at the phase speed of the waves. The kinetic energy of the wave travels along the wave beam shown, which would be down and to the right for the right column. The right column of results was taken while looking at the waves generated on the wide side of the topography. Fig. 5a, c are looking at the wave generated on the medium side while Fig. 5 e, g are looking at the steep side generated wave. All tests were performed at similar N values, and thus the angle of propagation is similar in all tests. Comparing the two sides of each test to each other shows that despite the different topography dimensions facing that side, the beam is nearly identical and thus generated waves seem unaffected by local topography shape.

Interferences can be seen on both sides, such as the diagonal beams coming off the main beam in Fig.6a, b that are nearly identical. These most likely are reflections of secondary waves generated off the main wave and reflected off the free surface. Interferences occur as the wave breaks down and are higher order waves that we do not address in this paper.

The horizontal and vertical wavenumbers (k and m) of the wave can be found by taking the Fourier transform in space and then time of the ΔN^2 data. These were then averaged over time to get an average k and m of each test and are shown in Fig. 7. The x axis is k while the y axis is

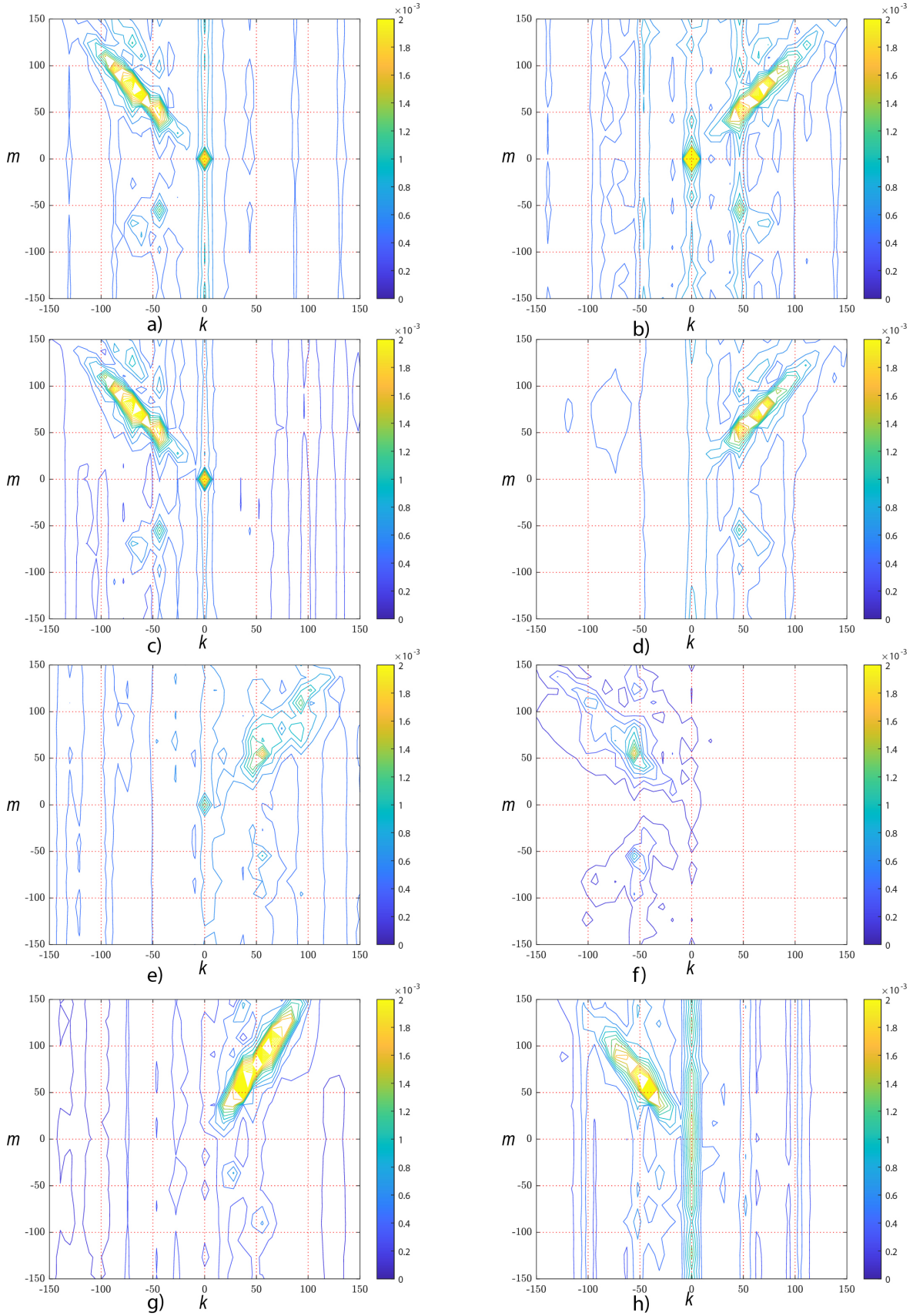

Fig. 7. Experimental k and m values for the generated waves for either side of the same topography, where the colors represent the Fourier amplitudes of ΔN^2

m and the plots are in the same order and correspond with Fig. 6. The contour colors show which wavenumbers contain the greatest amount of a form of energy, where yellow is the greatest. It is clear there are one to three peaks in each plot corresponding to three different possible k, m values. Fig. 7a) seems to show peaks at -50,-75, and -100 in k and 50, 75, and 100 in m. There is also some other energy that is generated at -50 k and -50 in m, which could correspond to turbulence generated waves or other interactions. Notice how the angles of the wave match again in every test and that the intensities match well when the two sides of the same tests are compared to each other. For a particular frequency (ω) and known k, due to the dispersion relation, m has only one possible value, thus the solutions are along a line at an angle to the vertical. However, especially on the wide side, in Fig. 7f, h the wave does not spread as high in k or m as the steep side of Fig. 7e,g. The wave in Fig. 7 e,g reaches near 100 in k and near 150 in m while in Fig. 7f,h the wave seems to die out at 75 in k and 100 in m, showing a possible difference in the generation of the waves due to the two different sides of the topography.

Exploring this difference further, a form of kinetic energy is estimated directly using the equation outlined in equation 10 and shown in Fig. 8. The x axis is k and the y axis is m while the color scale shows the kinetic energy where yellow indicates the greatest amount of energy. The plotted points are based on expected k and m which are calculated by

$$k_{exp} = \frac{2\pi}{L/2 + L_t} \tag{11}$$

$$m_{exp} = \sqrt{\frac{k_{exp} N^2}{\omega} - k^2} \tag{12}$$

where L is the excursion length and L_t is the width of the topography. There are three expected values plotted on each kinetic energy plot corresponding with the k_{exp} and m_{exp} of the side being imaged (side) the opposite side (opp) and the average between the two (avg). Fig. 8a,c shows that the wave generates energy mostly at the opposite and average wavenumber values, while there is still some energy at the side. However, on the wide side in Fig. 8 b,d there is very little energy at the opposite side, compared to the side and average. This indicates that not much energy is being generated by the medium side of the topography compared to the wide side. This is confirmed in Fig. 8e-h where the energy is concentrated at the opposite side when looking at the steep side, and the imaged side when looking at the wide images.

4 Conclusion

Although internal waves generated on each side of a two dimensional topography are visibly similar when generated by a single topography with different shapes on each side further quantitative analysis exposes some slight differences where the wave on the wide side of the topographies does not seem to reach the same amplitudes of k and m as the medium or steep sides do. The kinetic energy plots confirm this as on the wide sides there is less energy present at the higher values of k and m.

Due to the varied nature of underwater topography, the interaction between shape of topography and the generated wave must be understood. It has been demonstrated that there are valuable interactions between asymmetric topographies and the wave generated on either side of the topography that must be understood. Further tests and analysis will be conducted to explore these interactions and understand how the asymmetry of topographies affect internal wave generation.

References

[1] Nappo, C. J., 2013. *An introduction to atmospheric gravity waves*. Academic press.

[2] Lee, A., and Crockett, J., 2019. "Turning depths: Evanescent to propagating wave kinetic energy density". *Phys. Rev. Fluids,* **4**, Mar, p. 034803.

[3] Dalziel, S. B., Hughes, G. O., and Sutherland, B. R., 2000. "Whole-field density measurements by 'synthetic schlieren"'. *Experiments in Fluids,* **28**(4), 04/01, pp. 322–335.

[4] Peacock, T., Echeverri, P., and Balmforth, N. J., 2008. "An Experimental Investigation of Internal Tide Generation by Two-Dimensional Topography". *Journal of Physical Oceanography,* **38**, p. 235.

[5] Paoletti, M. S., Drake, M., and Swinney, H. L., 2014. "Internal tide generation in nonuniformly stratified deep oceans". *Journal of Geophysical Research: Oceans,* **119**(3), pp. 1943–1956.

[6] Laurent, L. S., Stringer, S., Garrett, C., and Perrault-Joncas, D., 2003. "The generation of internal tides at abrupt topography". *Deep Sea Research Part I: Oceanographic Research Papers,* **50**(8), pp. 987 – 1003.

[7] Legg, S., 2014. "Scattering of low-mode internal waves at finite isolated topography". *Journal of Physical Oceanography,* **44**(1), pp. 359–383.

[8] Grimshaw, R., and Helfrich, K. R., 2018. "Internal solitary wave generation by tidal flow over topography". *Journal of Fluid Mechanics,* **839**, p. 387–407.

[9] Echeverri, P., and Peacock, T., 2010. "Internal tide generation by arbitrary two-dimensional topography". *Journal of Fluid Mechanics,* **659**, p. 247–266.

[10] Pétrélis, F., Smith, S. L., and Young, W. R., 2006. "Tidal conversion at a submarine ridge". *Journal of Physical Oceanography,* **36**(6), pp. 1053–1071.

[11] Aguilar, D. A., and Sutherland, B. R., 2006. "Internal wave generation from rough topography". *Physics of Fluids,* **18**(6).

[12] Lee, F. M., Allshouse, M. R., Swinney, H. L., and Morrison, P. J., 2018. "Internal wave energy flux from density perturbations in nonlinear stratifications". *Journal of Fluid Mechanics,* **856**, p. 898–920.

[13] Hill, D. F., 2002. "General density gradients in general

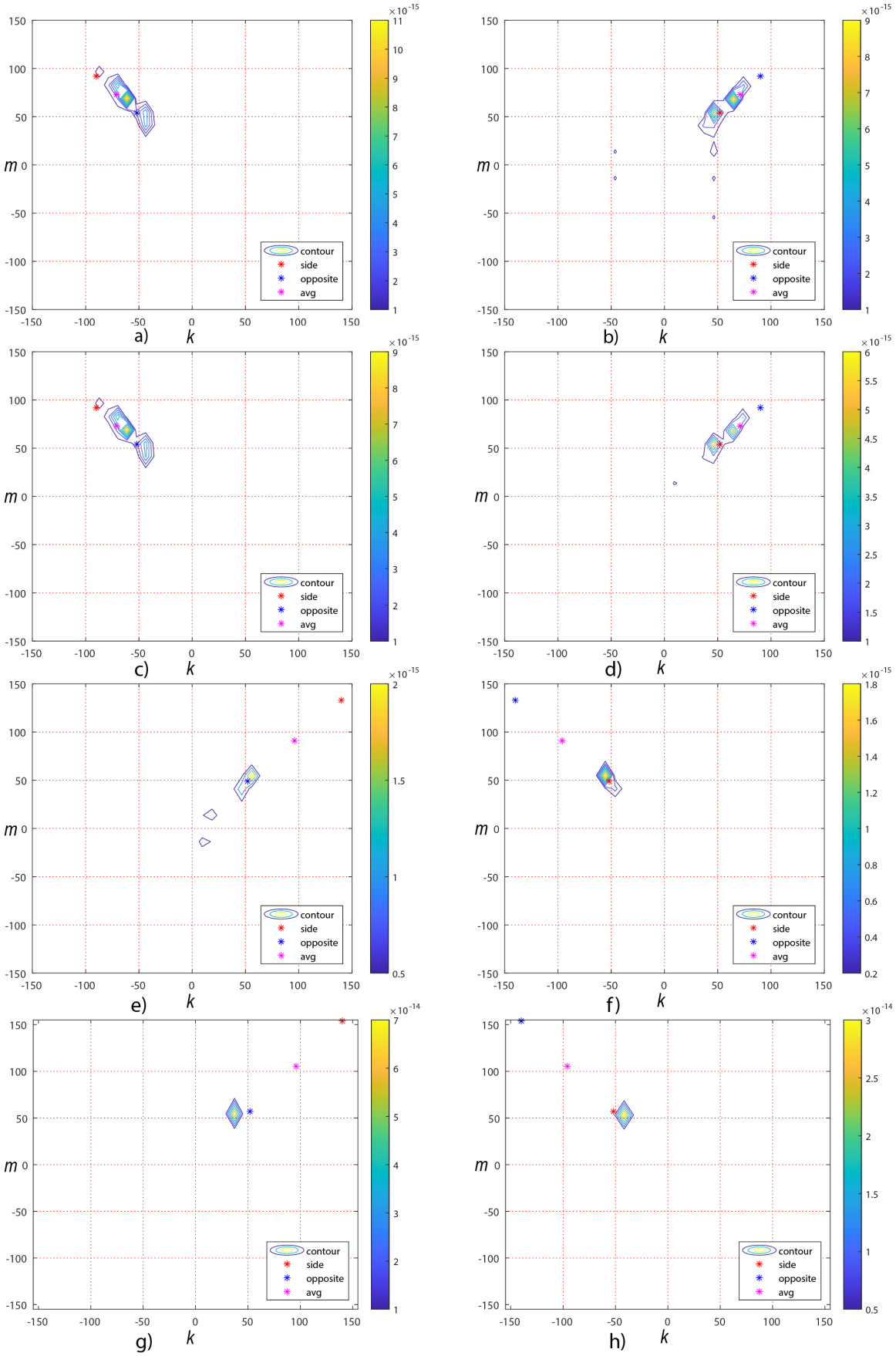

Fig. 8. Experimental kinetic energy values for the generated waves for either side of the same topography, where the colors represent the kinetic energy of the waves

domains: the “two-tank” method revisited”. *Experiments in Fluids,* **32**(4), pp. 434–440.

[14] Wunsch, S., and Brandt, A., 2012. “Laboratory experiments on internal wave interactions with a pycnocline”. *Expts. in Fluids,* **53**, pp. 1663–1679.